Egypt. J. Phys. **Vol. 51,** pp. 1-19 (2023)

Egyptian Journal of Physics

https://ejphysics.journals.ekb.eg/

Preparation, Characterization, Optical and Electrical Properties of Polyvinyl alcohol/Chitosan Blend Doped with Manganese Bromide for Electronic Applications

Emad Mousa and Galal H. Ramzy*

Physics Department, Faculty of Science, Cairo University, Giza, 12613, Egypt

Physics Department, Faculty of Science, Cairo University, Giza, 12613, Egypt

Abstract

Polyvinyl alcohol/chitosan (PVA/Cs) blend filled with the metal-salt manganese bromide ($MnBr_2$) was prepared using the solution-casting method. The effect of incorporating $MnBr_2$ on the electrical properties of the blend was investigated, with special reference to the effect of dehydration on the dielectric properties. Samples were characterized using XRD, SEM,TGA, and optical studies. Complexation between polymer blend and $MnBr_2$ is confirmed using XRD and optical analysis. A strong absorption band at 5.9 eV (210 nm) and a shoulder-like peak at 4.1 eV (305 nm) were found and explained. In addition, a blue shift is observed for the 305 nm band by the addition of $MnBr_2$ to the blend which confirmed the complexation between $MnBr_2$ and the PVA/Cs blend as predicted earlier by XRD data. In addition, $MnBr_2$dopedcomposites show higher thermal stability than the pure blend. Complex dielectric constant values are higher than similar (PVA/Cs) blend-metal salt composites reported in the literature.

Keywords:: Polymer composites, manganese bromide, optical properties, dielectric properties.

1. Introduction

Recently, the accumulation of synthetic plastic wastes in the environment reached a global scale of pollution that affects both wildlife as well as human populations [1]. Considering the prohibitive cost of removing the plastic pollutants from our planet, one of the feasible solutions in this regard is to use biodegradable plastics instead [2].

Among polymers, polyvinyl alcohol (PVA) is a hydrophilic, safe, synthetic polymer of excellent properties. It is characterized by high dielectric strength, acceptable charge storage ability, and is highly elastic [3]. In addition, PVA has excellent adhesive properties and film-forming ability by casting with high chemical resistance against organic solvents [4].

Although PVA is a biodegradable polymer, it is biologically inactive. Indeed, the antibacterial activity of PVA could be induced by the addition of the natural polysaccharide chitosan polymer [5]. On the other hand, blending with chitosan lowers the optical transparency of PVA while increasing its tensile strength and decreasing its elongation at break [6].

However, PVA/Cs is a very common biodegradable blend that is used in a variety of applications. Despite being widely used in controlled drug release [7] many researchers studied the use of this blend in other applications such as fibroblast adhesion in biomedical applications [8], selective sorption of environmental contaminants from aqueous solutions [9], and polymeric packaging films for specific purposes [6].

*Corresponding author: *e-mail: galalramzy@cu.edu.eg

DOI : 10.21608/EJPHYSICS.2022.146907.1081

Received: 28/6/2022; accepted: 9/8/2022

Adding fillers to polymers does not only improve and stabilizes their performance but also enlarges their field of applications [10]. Few trials to improve the conductivity of PVA/Cs blend by addingdifferent ionic salts were studied by few researchers [11, 12].

Earlier studies emphasized that incorporating metallic salts into organic polar polymers may alter their physical properties [13–15]. Although lithium salts are used mainly in storage battery applications, bivalent metal salts are more advantageous for non-battery devices since they are less reactive than monovalent metal salts [16].

To the best of our knowledge,manganese (II) bromide tetrahydrate salt ($MnBr_2.4H_2O$), which is an ionic crystalline salt, has never been studied as a dopant in polymers.

In the present work, $MnBr_2.4H_2O$ is added to PVA/Cs blend as a filler prepared using casting method. XRD, SEM and TGA techniques were used to characterize the samples. Both DC and AC electric properties of the composites will be investigated.

2. Experimental

2.1. *Film preparation*

Transparent polymeric films were prepared using thesolution casting method. All chemicals were used as received without any further treatments.

Two grams of chitosan (Sigma Aldrich, shrimp source chitosan, deacetylation degree ≥75%) was dispersed in 100 ml of double-distilled (DD) waterand stirred for 30 minutes. 1 ml of acetic acid (Merk, glacial 100%, pro analysis) was added to the aqueous solution of chitosan and stirred vigorously for 24 h at ambient temperature to form chitosan acetate. 2 g of PVA powder (Fluka, average molecular weight 72000, 98% hydrolysis) were dissolved in 50 ml of DD water and stirred for 45 minutes at 90 ^{o}C. The solution was allowed to cool down to ambient temperature for an additional 1 h with mild stirring.

The PVA solution was added dropwise to the Cs solution, with continuous stirring, in a ratio of (50/50wt) PVA/Cs and stirred for an additional 3 h at ambient temperature. The procedure is shown schematically in Fig. 1.

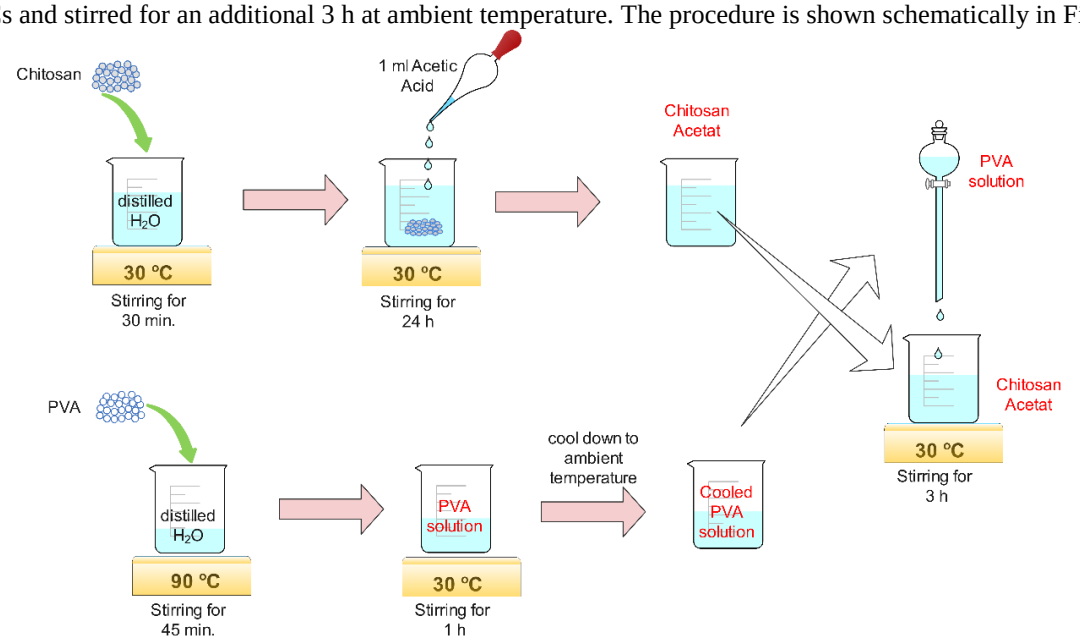

Fig. 1. Schematic preparation of (50-50 wt %) PVA/Cs blend

For the preparation of composite films, 1 g of $MnBr_2$ (Sigma Aldrich, Manganese II Bromide tetrahydrate, 98%) was dissolved in 15 ml of DD water at ambient temperature. The $MnBr_2$ solution was added in different weight proportions (1 %, 3 %, and 5 %) to the blend solution and stirred for 1 h. Solutions were pouredinto Pyrex

..
Petri dishes and allowed to dry in an electrical oven 40 ^{o}C for 48 h. Films were peeled off the Petri dishes and stored inside a glass desiccator.

2.2 Characterization

The x-ray diffractometer (Empyrean, Malvern Panalytical Company) was used to record the X-ray diffraction patterns of the prepared films. Measurements were conducted at ambient temperature with copper-target K_{α} radiation (λ = 0.154 nm). Samples were scanned from 5^{o} to 90^{o} (2θ) at a rate of 1^{o}/min (step-size of 0.013^{o}).

Field Emission Scanning electron microscope (FE - SEM; Quanta 250 Field Emission Gun, Netherlands) was used to analyze the morphology of all samples. Prepared films were freeze-dried and fractured under liquid nitrogen for cross-section observation. A sputter coater (K550X, EMITECH, England) was used to pre-coat conductive gold onto the fracture surfaces before scanning.

Thermogravimetric analyses (TGA) were carried out from ambient temperature to 600 ^{o}C (rate = 10 ^{o}C/min) using a Shimadzu TG-50H thermal analyzer.

2.3 Measurements

Optical investigation was done using a (UV-3600 Plus, Shimadzu) spectrophotometer in the wavelength range of 200-2500 nm (step size= 5 nm).

For electrical measurements, samples were cut in the form of discs with a thickness of 0.2 mm and a diameter of 1 cm. In addition, samples were coated with a conductive silver paste to ensure the contact electrode will have an Ohmic contact with the specimens.

DC measurements of electrical conductivity were recorded using a digital electrometer (KEITHLEY 6517A AUTORANGING ELECTROMETER, USA). A temperatureramp was carried out at a rate of 1 ^{o}C/min in the range (30 ^{o}C – 140 ^{o}C).

AC dielectric measurements were analyzed using a computer-controlled LCR bridge (HIOKI, 3532-50 LCR Hi-TESTER, JAPAN) in the frequency range 50 Hz – 5 MHz. To study the effect of dehydration on dielectric properties, samples were heated up to 140 ^{o}C at a rate of 1 ^{o}C/min and then left to cool down under vacuum to ambient temperature before starting the measurements.

3. Results and Discussion

3.1 X-Ray Diffraction (XRD)

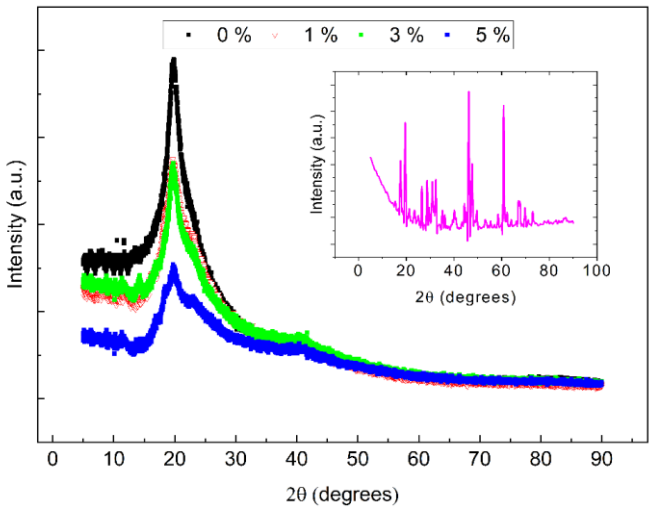

Fig. 2. XRD pattern of pure PVA/Cs blend and its (1 %, 3 %, and 5 %) $MnBr_2$ loaded composites. Inset figure represents XRD pattern of pure $MnBr_2$.

Figure 2 represents the XRD spectrum of PVA/Cs blend and its $MnBr_2$ (0, 1, 3, and 5 wt%) loaded composites, while the inset of Fig. 2 shows the XRD pattern of pure manganese bromide tetrahydrate $MnBr_2.4H_2O$. CHECKCELL program was used to index and analyze the diffraction peaks of $MnBr_2$[17]. The

analysis revealed a monoclinic structure ($P2_1/n$) with lattice parameters, a = 11.668 Å, b = 9.824 Å, c = 6.316 Å, and the volume of the unit cell 714.2 $Å^3$ in agreement with the literature [18].

Obviously, only one broad diffraction peak for pure PVA/Cs blend, appeared in the x-rays chart that originates from PVA as reported in the literature [19]. The crystalline peak is centered at 19.6^o and superimposed on a broad hump (14^o – 30^o) that reflects the amorphous content of the blend.The elimination of the hydrated structure of chitosan could be due to the interactions between PVA and chitosan via hydrogen bonding [20].

For all composite films the diffraction peaks corresponding to $MnBr_2$ were absent. Moreover, the intensity of the peak at 19.6^o decreases as the concentration of $MnBr_2$ increases.

Hodge et al. [21]suggested that the polymeric blend transfers from a semicrystalline structure to an amorphous structure as the metal salt disrupts the polycrystalline structure of the blend. This ensures the dissolution of manganese bromide in the amorphous regions, and complexation between $MnBr_2$ and the polymer blend occurs[22]. Such behavior is close to that observed in similar materials [23, 24].

3.2 SEM Characterization

Cross-sectional SEM micrographs of PVA/Cs composites loaded with different concentrations of $MnBr_2$ are illustrated in Fig. 3 (a–d). A homogenous dense micrograph is observed for the pure PVA/Cs blend which confirms the miscibility of PVA and chitosan. This is probably because chitosan tends to be embedded adherently in the pores of PVA [25].

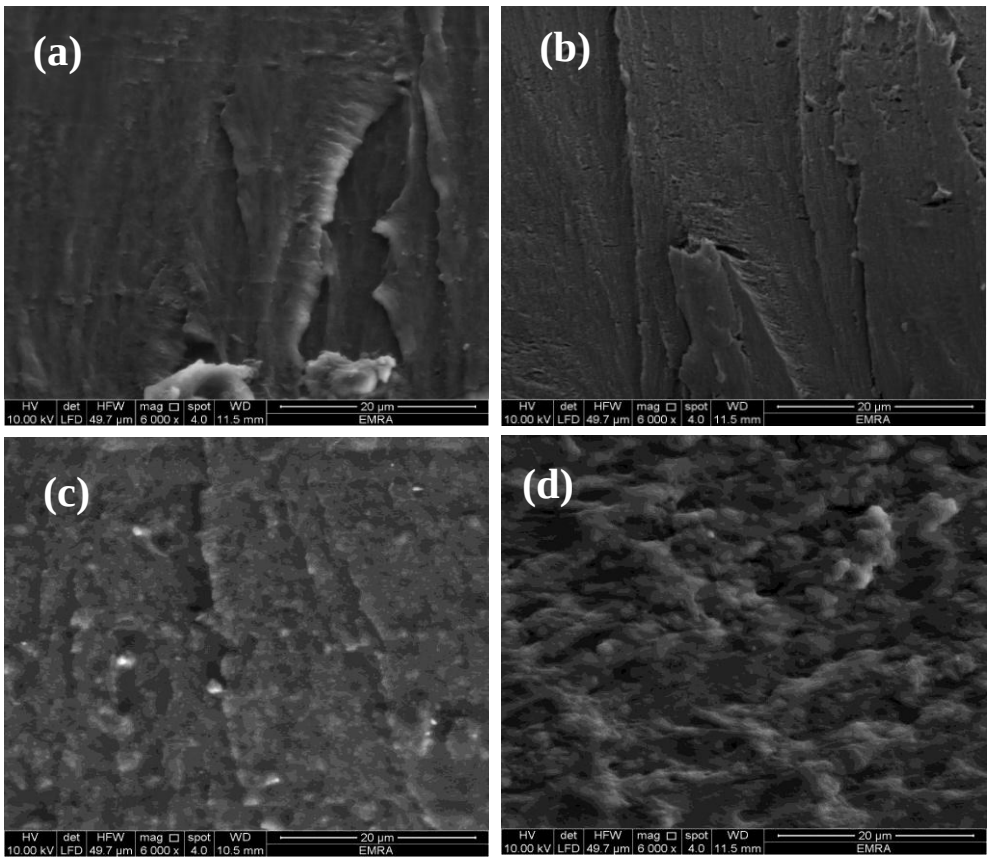

Fig. 3. SEM images of magnification 6000x for (a) pure PVA/Cs blend (b) 1% (c) 3% and (d) 5% of $MnBr_2$ incorporated with PVA/Cs.

Moreover, it is obvious that there is no evidence of agglomeration of the $MnBr_2$in the micrographs of composite films indicating that the filler particles are homogeneously distributed in the host matrix.

..

3.3 Thermal Analysis (TGA)

TGA thermograms of all samples in the temperature range (30 – 600 °C) are shown in Fig. 4. Few decomposition regions can be seen in the TGA curve of the unloaded PVA/Cs blend. The first process below 200 °C owes to the vaporization of moisture and adsorbed water [26]. The weight loss in this process increases by increasing the $MnBr_2$ content due to the dehydration of $MnBr_2.4H_2O$ salt.

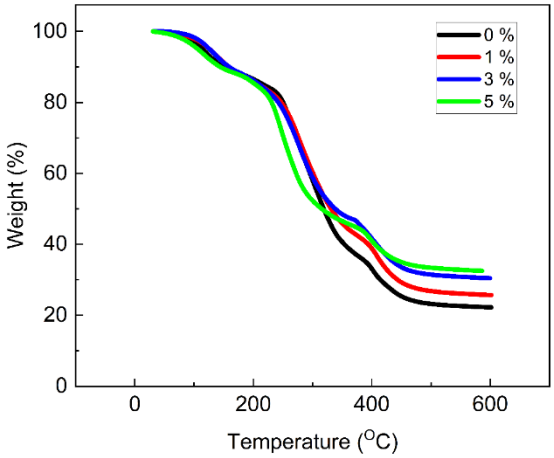

Fig. 4. Thermograms of pure PVA/C*s* blend and its (1%, 3%, and 5%) $MnBr_2$ loaded composites.

In addition, the primary thermal decomposition process lies between 200 – 450 °C and is followed by char formation at 480 °C. In fact, the major decomposition process shows a fairly pronounced knee at 400 °C which belongs to the PVA content in the blend [27-28]. This originates from the fact that thermal degradation of PVA takes place in two separate processes including aldehydes and formation of ketones at 250 – 350 °C, and the production of alkenes, alkanes, and unsaturated or aromatic hydrocarbons at 400 – 450 °C [28]. Meanwhile, the decomposition of Chitosan's' acetylated and deacetylated units and dehydration of saccharide rings were reported in a single process at 250 – 350 °C [19].

For the decomposition process at 250 – 350 °C, a decrease in the weight loss is observed with the increase in $MnBr_2$ concentration. This can be attributed to the increase in chain mobility in the amorphous regions induced by the addition of $MnBr_2$. Furthermore, the residual weight (char) of $MnBr_2$ loaded samples is higher than the pure PVA/Cs blend and increases with the increase in $MnBr_2$ content.

The temperature at which each sample has lost 50% of its original weight ($T_{50\%}$) is higher for all composites than a pure blend which reflects higher thermal stability of composites. Table 1 summarizes the residual weight at 600 ^{o}C, ($T_{50\%}$), and weight losses for each process.

The thermal decomposition' activation energy may be estimated using Broido equation [29]:

$$\ln\left[\ln\left(\frac{1}{\gamma}\right)\right] = -\frac{E_a}{R}\frac{1}{T} + C \qquad (1)$$

where R (8.314 J/mol.K) is the universal gas constant, T is the temperature in kelvins, E_a is the activation energy, and γ is the fraction of the residual material given by

$$\gamma = \frac{w_r - w_f}{w_i - w_f} \qquad (2)$$

where w_i, w_f and w_r are the initial weight of the sample, final weight, and residual weight at temperature T, respectively.

The activation energies for all samples could be determined from the slope of (ln[ln (1/γ)]) versus (1/T) plots (not presented here) using the expression (E_a = - R × slope). All data were carefully fitted to equation (1) with R^2

≥ 0.987. .Small changes in E_a values of composites with respect to the blend excludeany bond weakening effects in the blend after complexation with $MnBr_2$. Extracted E_a values are listed in Table 1.

TABLE 1. TGA parameters

$MnBr_2$ content (wt%)	$T_{50\%}$ (^oC)	Residue at 600 ^oC (wt%)	Decomposition steps		
			Temperature range	**Losses (wt%)**	**E_a (kJ/mol)**
0%	319	22.2	80 ^oC – 148 ^oC	10	42.8
			240 ^oC – 351 ^oC	43	41.6
			394 ^oC – 469 ^oC	10	36.5
1%	328	25.7	90 ^oC – 160 ^oC	10	41.6
			236 ^oC – 343 ^oC	36	44.9
			390 ^oC – 478 ^oC	13	43.2
3%	337	30.4	92 ^oC – 163 ^oC	11	52.4
			222 ^oC – 330 ^oC	32	41.2
			370 ^oC – 479 ^oC	15	42.3
5%	326	32.6	88 ^oC – 164 ^oC	12	50.7
			218 ^oC – 327 ^oC	35	56.5
			394 ^oC – 485 ^oC	11	38.2

3.4 Optical properties

In the current section, the behavior of the transmittance T and the reflectance R of investigated samples in UV-Vis region (200 – 700 nm) will be discussed.

3.4.1 Reflection and transmission spectra

The transmission spectra for all specimens are presented in Fig. 5, whereas the reflection spectra are presented in Fig. 6. Obviously, the transmission decreases as the content of $MnBr_2$increases, in the UV region up to 450 nm. Such behaviour reveals the higher absorption of $MnBr_2$ loaded samples resulting from electronic transitions. But, at higher wavelengths (Vis -region) the transmittance of pure blend was the lowest. Meanwhile, the reflectance decreases upon loading $MnBr_2$ in the PVA/Cs matrix over the whole scanned wavelength range.
The transparency of a sample is derived from the relation [30]:

$$Transparency = \frac{1}{t} log\,(T\%)_{600} \qquad (3)$$

where $(T\%)_{600}$ is the percent transmittance at 600 nm, and t is the film's thickness.

The transparency of all samples was plotted against the $MnBr_2$ concentration in the inset of Fig. 5. Slight variations in the transparency of the samples were observed. However, semicrystalline regions in the pure PVA/Cs matrix act as dispersive phases that lead to hazy film [31]. The induced amorphousity caused by the initial addition of $MnBr_2$ (1 % wt) led to a relative increase in transparency. Further addition of $MnBr_2$ (3 % and 5 %) enhances the light absorption by the dopant itself and causes a relative decrease in transparency.

..

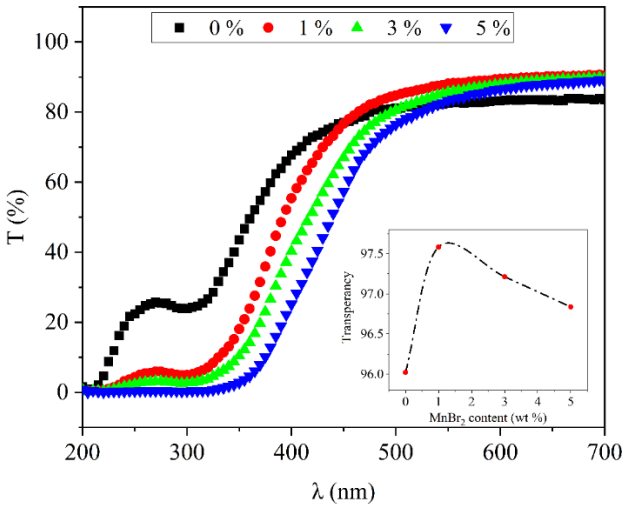

Fig. 5. Transmission spectra of pure PVA/Cs blend and its (1%, 3%, and 5%) $MnBr_2$ loaded composites. Inset figure represents transparency as a function of $MnBr_2$ content.

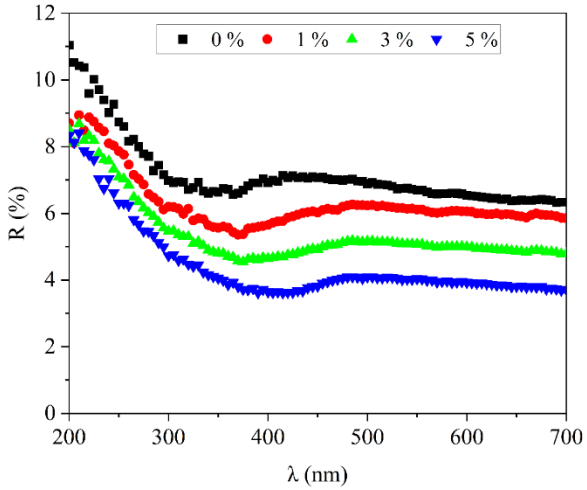

Fig. 6. Reflection spectra of pure PVA/Cs blend and its (1%, 3%, and 5%) $MnBr_2$ loaded composites.

3.4.2 Absorption studies

Optical absorption in the (UV – Vis) regions is anessential method to study the electronic properties of polymers [32].Knowing the reflectance *R* and transmittance *T* at a certain wavelength λ, the absorbance *A* at this wavelength can be determined using the relation [33]:

$$A = \ln\left(\frac{(1-R)^2 + \sqrt{(1-R)^4 + 4R^2T^2}}{2T}\right) \qquad (4)$$

Obviously, in Fig. 7, the absorption spectra (*A* versus λ) showncan be divided into three main regions namely, high absorption region ($\lambda \leq$300 nm), absorption region (300 nm $\leq \lambda \leq$ 500 nm), and transparent region ($\lambda \geq$ 500 nm).

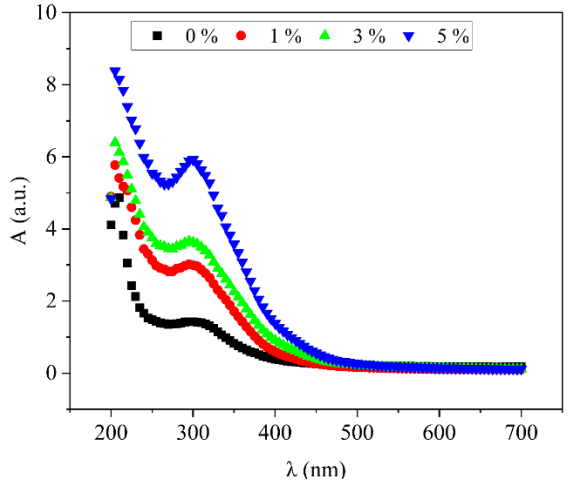

Fig. 7. Absorption spectra of pure PVA/Cs blend and its (1%, 3%, and 5%) $MnBr_2$ loaded composites.

The absorption spectrum of pure PVA/Cs blend shows two absorption bands in the UV region. A strong absorption band at 5.9 eV (210 nm) belongs to the unsaturated ethylene group as well as the carbonyl group present in PVA [34], and a shoulder-like peak at 4.1 eV (305 nm) is attributed to the chromophoric groups present in chitosan namely, N-acetylglucosamine and glucosamine [26, 35]. In addition, a blue shift is observed for the 305 nm band by the addition of $MnBr_2$ to the blend which confirms the complexation between $MnBr_2$ and the PVA/Cs blend as predicted earlier by XRD data.

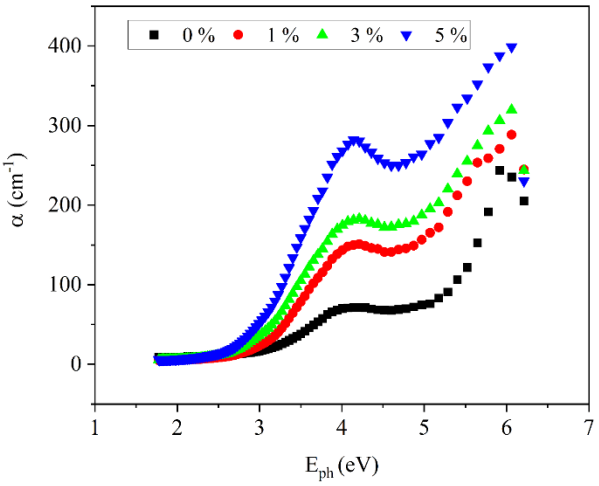

Fig. 8. Energy dependence of the absorption coefficient for PVA/CS samples of different $MnBr_2$ content.

The absorption coefficient α is plotted *vs* the incident photon energy E_{ph} in Fig. 8. However, the transitions of electrons between the valence band and the conduction band are reflected in the absorption spectra as a sharp increase in the absorption at the edge [36]. Recall that the absorption edge is the photon's energy above which the absorption increases abruptly, the intercept value with E_{ph}- axis corresponds to the value of the absorption edge E_e.

The mode of interband transitions can be determined at higher values of α by Tauc[37] and Mott and Davis [38] models:

$$\alpha E_{ph} = B_t (E_{ph} - E_g)^m \qquad (5)$$

where B_t is the band tail parameter and is related to transition probability, E_g is the optical band gap energy between the highest maximum of the valence band and the lowest minimum of the conduction band, and (m = 1/2, 3/2, 2, 3) is the factor which represents direct allowed, direct forbidden, indirect allowed, and indirect forbidden optical transition modes, respectively.

..

Plots of $(\alpha E_{ph})^2$ and $(\alpha E_{ph})^{1/2}$ against E_{ph} are illustrated, respectively, in Fig. (9a) and (9b). Direct band gap $E_{g(d)}$ and indirect band gap $E_{g(i)}$ values are deduced from the intersection of the linear portion of the high absorption region with x-axis in Fig. (9a) and (9b), respectively. Accordingly, calculations showed that both $E_{g(d)}$ and $E_{g(i)}$ decrease with the increase in $MnBr_2$ content. Obviously, $E_{g(d)}$ decreases by 20% from 5.5 eV to 4.4 eV upon loading 5% (by weight) of $MnBr_2$ in the PVA/Cs matrix, while $E_{g(i)}$ decreases by 52.2% from 4.6 eV to 2.2 eV. This finding suggests that indirect electronic transitions in the examined samples are more probable than direct ones [37, 39].

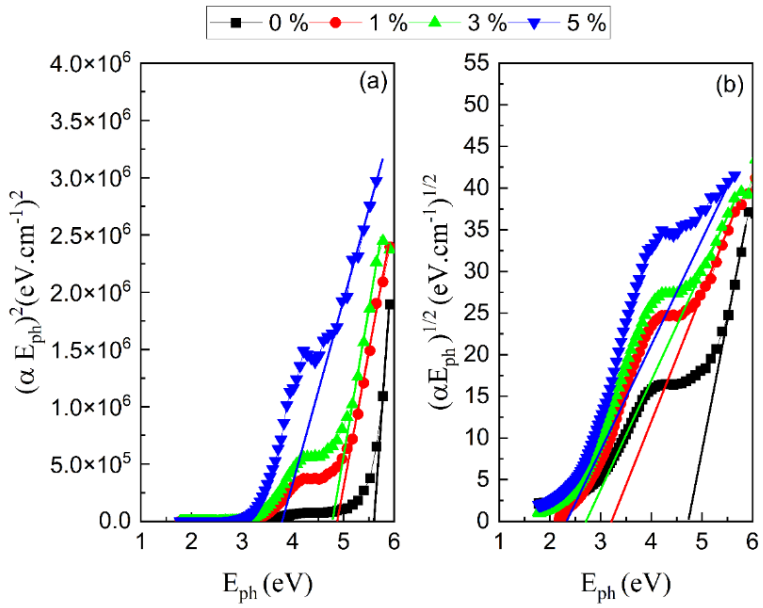

Fig. 9. Variation of $(\alpha E_{ph})^2$ and $(\alpha E_{ph})^{1/2}$ as a function of incident photon energy (E_{ph}) for PVA/Cs samples of different $MnBr_2$ content.

The absorption coefficient in the (low – moderate) absorption region, follows Urbach equation [40]:

$$\alpha = \alpha_i \exp\left(\frac{E_{ph}}{E_b}\right) \qquad (6)$$

where α_i is a constant and E_b is the band tail width (Urbach energy) of the localized states in the band gap.

The Urbach energy E_b is deduced from the reciprocal of the slope of fitting straight - line of l n α *vs* E_{ph} represented in Fig. 10.

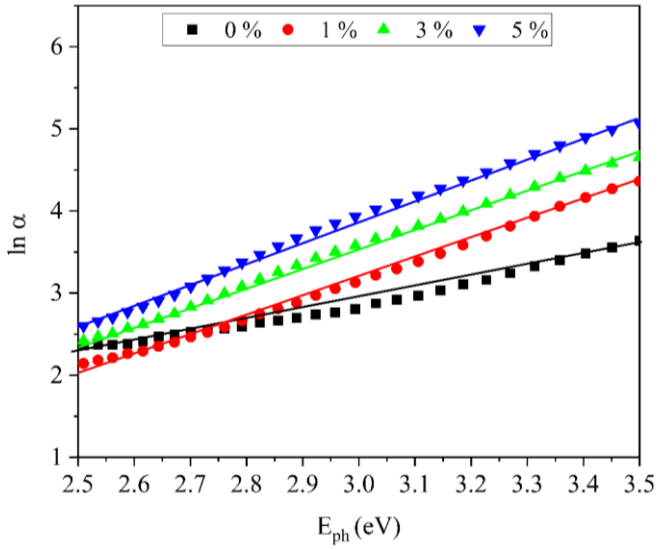

Fig. 10. Variation of (ln α) as a function of incident photon energy (E_{ph}) for PVA/Cs samples of different $MnBr_2$ content. Solid lines represent theoretical fit.

Values of E_e, E_g, and E_b are listed in Table 2. The energy gap decreases from 5.4 eV to 4.7 eV upon loading of $MnBr_2$ in the composites. This may be explained in terms of formation of new donor levels in the forbidden zone [41]. Also, the values of E_b decrease by increasing the $MnBr_2$ content owing to the disorder induced in the PVA/Cs matrix [42].

The extinction coefficient K is used properly to describe the extent of damping (absorption loss) of electromagnetic waves inside the material [43].

$$K = \frac{\alpha\lambda}{4\pi} \qquad (7)$$

TABLE 2. Optical parameters

$MnBr_2$ content (wt%)	E_e (eV)	$E_{g(d)}$ (eV)	$E_{g(i)}$ (eV)	E_u (eV)
0 %	5.2	5.5	4.6	1.1
1 %	3.9	5	3.2	1.3
3 %	3.7	4.8	2.7	1.7
5 %	3.1	4.4	2.2	2.1

The spectral dependence of the extinction coefficient K is illustrated in Fig. (11). Over the whole wavelength' range (200 – 700 nm), the values of K were very small (of order 10^{-4}) indicating that the samples under investigation are insulators at ambient temperature [43]. The inset of Figure (11) represents K at 600 nm as a function of $MnBr_2$ content. Clearly, ,K behaves in a reversible manner to transparency. The absorption is higher for the pure PVA/Cs blend and decreases with the amorphousity induced by addition of $MnBr_2$ (1 %) to the blend, and finally increases upon increasing the amount of the dopant (3 % and 5 %) as discussed earlier.

..

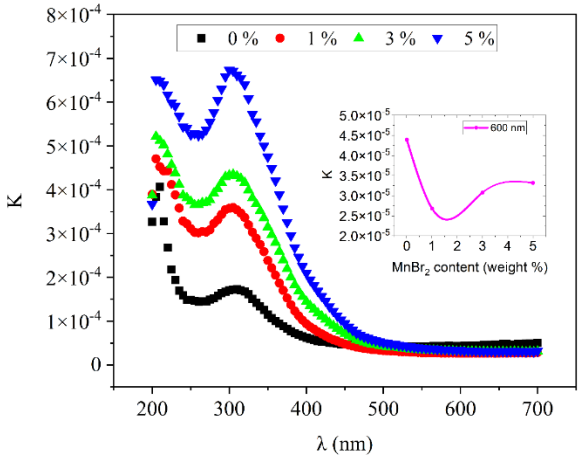

Fig. 11. Spectral dependence of the extinction coefficient (*K*) for different contents of $MnBr_2$ loaded samples. Inset figure represents (*K*) as a function of $MnBr_2$ content at 600 nm.

3.5 Electrical properties

3.5.1 DC electrical conductivity

The temperature dependence of DC conductivity may be predicted by the Arrhenius equation:

$$\sigma = \sigma_o \exp\left(-\frac{\Delta E_{dc}}{k_B T}\right) \qquad (8)$$

where σ_o is a factor, k_B is the Boltzmann constant ΔE_{dc} is the activation energy, and T is the absolute temperature.

Figure 12 depicts ln (σ_{dc}) *vs* (1000/*T*) plots for PVA/Cs matrix loaded with different $MnBr_2$ loadings. The observed DC conductivities for all samples attain two thermally activated regions separated by a negative slope region (90 ^{o}C – 120 ^{o}C). The increased free volume upon thermal expansion of samples results in increasing the mobility of charge carriers and consequently leads to an increase in conductivity [44]. Taking into consideration the different rates of heating in TGA and electrical measurements, the negative slope region is suggested to be accompanied with the dehydration process. The initial loss of free water molecules led to a decrease in conductivity until samples are thermally stabilized after complete water evaporation [45].

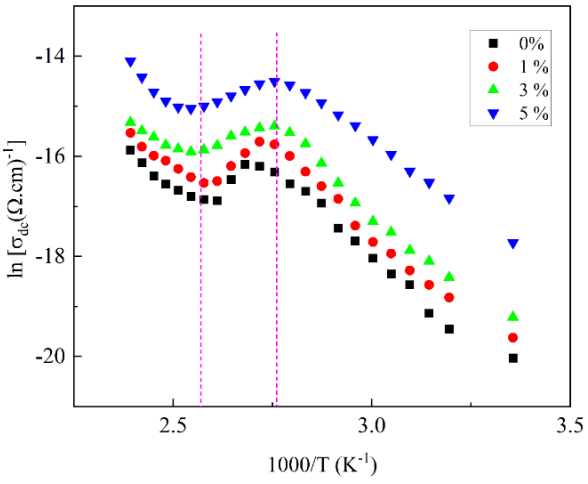

Fig. 12. Temperature dependence of the DC conductivity for PVA/Cs samples of different $MnBr_2$ content.

However, the DC conductivity values at ambient temperature as well as the activation energy values in the two thermally activated regions are summarized in Table 3. The conductivity of pure PVA/Cs blend at ambient temperature increased from 1.9×10^{-9} to 2.1×10^{-8} $(\Omega.cm)^{-1}$ for the 5% $MnBr_2$ loaded sample.

TABLE 3. Parameters extracted from DC measurements

$MnBr_2$ content (wt%)	ΔE_{dc} (eV)		σ_{dc} $(\Omega.cm)^{-1}$ at 30 °C
	region I	**region II**	
0 %	0.58	0.59	1.9×10^{-9}
1 %	0.57	0.49	3.1×10^{-9}
3 %	0.58	0.39	4.5×10^{-9}
5 %	0.49	0.66	2.1×10^{-8}

3.6 Dielectric analysis

3.6.1 Untreated samples

The measured impedance *Z* of the samples was resolved into two components: the real component Z' and imaginary component Z'' at different frequencies. Nyquist plots of Z'*vs* Z'' of PVA/Cs samples loaded with different concentrations of $MnBr_2$ at ambient temperature are illustrated in Fig. (13).

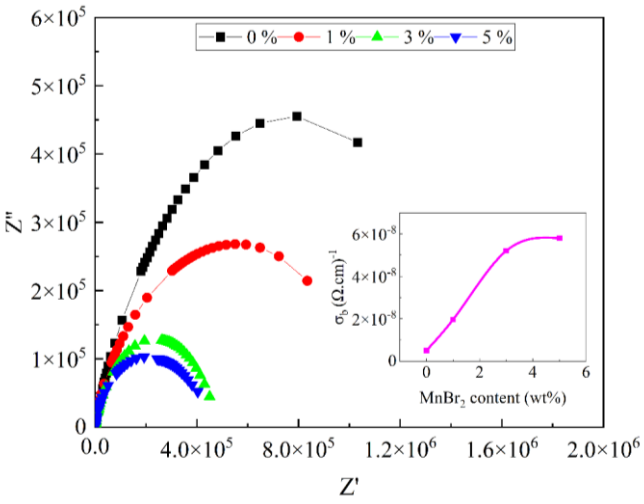

Fig. 13. Nyquist plots for PVA/Cs samples of different $MnBr_2$ content. Inset figure represents (σ_b) as a function of $MnBr_2$ content.

All plots are characterized by single semicirculararcs whose centers lie below the Z'- axis and decrease with the increase in $MnBr_2$ concentration. The semicircular plots pass through the origin at high frequency suggesting an equivalent circuit consists of a bulk resistor R_b connected in parallel with a (frequency-dependent) capacitor C_b. The bulk resistor represents the motion of ions through the free volume of the polymer matrix, whereas the capacitor represents the polarized immobile polymeric chains in the alternating field [46].

However, R_b can be derived from the intersection of the semicircular arc with the Z'- axis. The bulk conductivity (σ_b) can be found using the relation $\left(\sigma_b = \frac{t}{A}\frac{1}{R_b}\right)$, where *t* and *A* are the thickness and area of the sample respectively. The inset of Fig, (14) shows an increase inσ_b with the increase in the content of $MnBr_2$. This can be attributed to the increase in the mobilityof the charge carriers [47].

The total conductivity (σ_{total}) of a solid, derived from the measured conductance $\left(G = \frac{A}{t}\sigma_{total}\right)$, is the sum of its AC and DC conductivities. The frequency dependence of measured conductivity for different $MnBr_2$ loaded samples at ambient temperature is shown in Fig. 14. A DC plateau region appears at low frequency for all samples and its width increases as the $MnBr_2$ content increase. Meanwhile, the conductivities beyond the plateau region increase with the increase in frequency and tend to merge at high frequencies. An insulator to semiconductor transition takes place upon increasing the frequency for all samples (~ 10^{-9} $\Omega^{-1}.cm^{-1}$ – 10^{-6} $\Omega^{-1}.cm^{-1}$). The conductivity of all samples obeys the universal dynamic response ($\sigma_{ac}(\omega) \propto \omega^S$). where, σ_{ac} is the AC conductivity at a particular temperature and frequency ω, and ($0 < S < 1$) is a power factor [48].

..

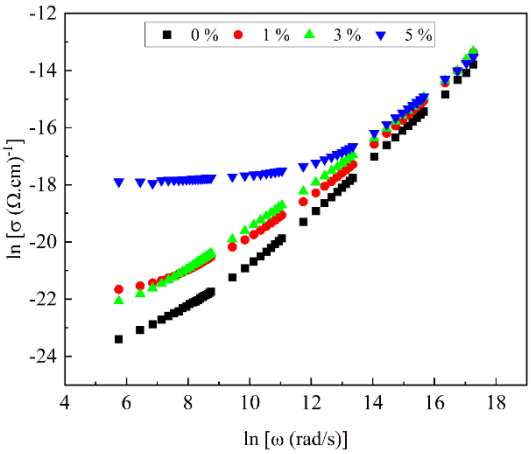

Fig. 14. Frequency dependence of the total conductivity for PVA/Cs samples of different $MnBr_2$ content.

The real part ε' which represents the dielectric constant and imaginary part ε'' which is loss factor of the dielectric permittivity ($\varepsilon^* = \varepsilon' - i\,\varepsilon''$) have been derived from the measured impedance values according to the following equations [49]:

$$\varepsilon' = \frac{t}{\omega \varepsilon_o A}\frac{Z''}{Z^2} \qquad (9)$$

$$\varepsilon'' = \frac{t}{\omega \varepsilon_o A}\frac{Z'}{Z^2} \qquad (10)$$

where ε_o is the permittivity of free space.

The frequency dependence of the dielectric constant ε' for all samples at ambient temperature are plotted in Fig. 15. Many conclusions may be extracted from this figure.

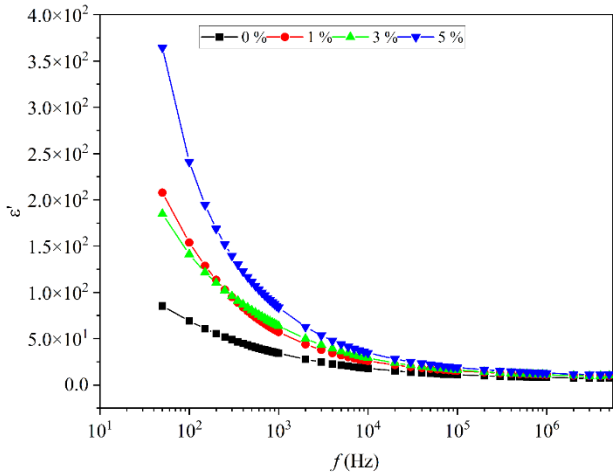

Fig. 15. Frequency dependence of the dielectric constant (ε') for PVA/Cs samples of different $MnBr_2$ content.

Firstly, ε' decreases gradually with increasing frequency and attains a constant value at higher frequencies. Similar behaviors were observed in many other polymer systems [50]. At low frequencies, permanent and induced dipoles have a sufficient time to align themselvesalong the electric field' direction leading to higher value of the dielectric constant. At higher frequencies, the polarization lags the electric field leading to a lower value of dielectric constant [51].

Secondly, the value of ε' for the pure PVA/Cs blend at 100 Hz and 30 ^{o}C is 69, which is higher than that reported for both pure chitosan and pure PVAin literature [52, 53]. In fact, the dipoles in pure polymers originate mainly from the main chain, side groups, and molecular segments and other impurities formed as byproducts of the polymerization process. Meanwhile, an additional interfacial polarization at the boundaries of heterogeneous components was located in polymer blends. This may lead to an increase in the value of ε' than pure components unless the molecular conformations of the mixed constituents disrupt the net dipolar arrangement [54]. Moreover, it is worth noting that freely rotating dipoles have a greater participation rate in increasing the dielectric constant value than constrained ones. This may explain the role of water content in raising ε' value of the blend.

Finally, ε' of the composites increases with increasing the $MnBr_2$ concentration. Dopants may affect the$\varepsilon'$of a polymer composite depending on several factors such as the value of ε' of the dopant itself, the dopant concentration, the particle size of the dopant, and the type of interaction between the polymer and the dopant [55].

Figure 16 shows the dependence of the dielectric loss ε''on the frequency for all composites at ambient temperature. Unfortunately, the dielectric loss values of all samples are high (~ 10^3 at 100 Hz for 5% sample). The dielectric losses in polymers result mainly originate from distortional dipolar, interfacial, and conduction losses [56].

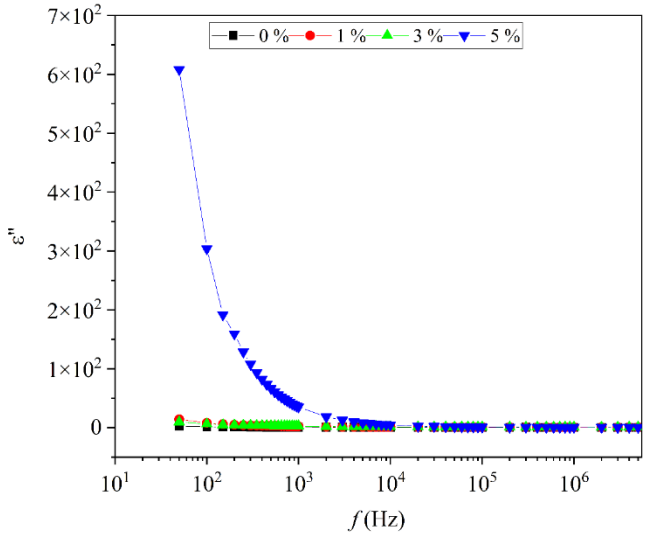

Fig. 16. Frequency dependence of the dielectric loss (ε'') for PVA/Cs samples of different $MnBr_2$ content.

..

3.6.2 Pre-heated samples

The frequency dependence ofσ_{ac} for dehydrated samples is illustrated in Fig. 17. A significant decrease in the values of σ_{ac} for all samples after dehydration of water is observed (10^{-9}- 10^{-11} $(\Omega.m)^{-1}$ at 100 Hz for pure blend). Also, it is obvious from Fig. 17 that a wide frequency independent plateau region appears at low frequency for the 5% $MnBr_2$ loaded sample, as an evidence of ionic conductivity domination of this concentration.

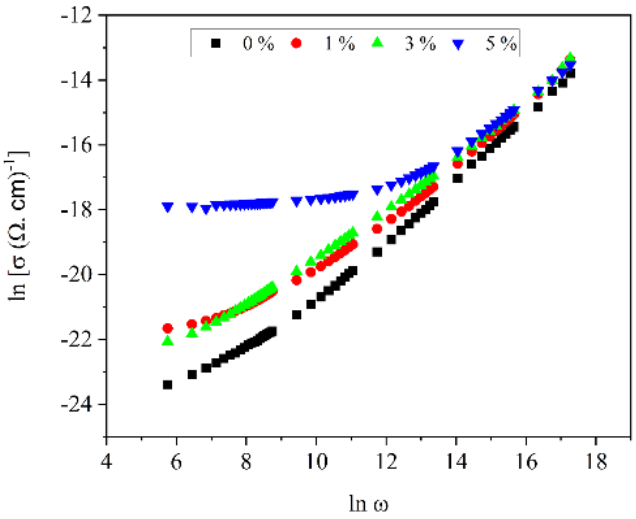

Fig. 17. Frequency dependence of the total conductivity for dehydrated PVA/Cs samples of different $MnBr_2$ content.

However, the decrease in AC conductivities upon dehydration of samples reflects a decrease in their dielectric losses ($\sigma_{ac}= \omega \varepsilon_o \varepsilon''$).

On the other hand, Fig. 18 shows the values of ε' for all samples as a function of frequency. An expected decrease in the dielectric constantε' for all samples is attained because of losing free water molecules. However, values of ε' at ambient temperature are still high (ε'= 24 at 100 Hz and 30 ^oC for 5% loaded sample) with respect to similar PVA/Cs blend-metal salt composites reported in literature [10]. These results suggest that dehydrated composites may be useful in high dielectric constant applications.

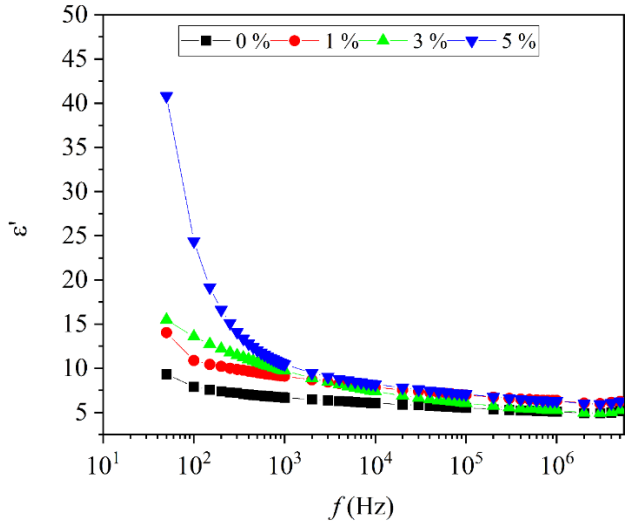

Fig. 18. Frequency dependence of the dielectric constant (ε') for dehydrated PVA/Cs samples of different $MnBr_2$ content.

Conclusions

Based on the above results, we can conclude that, complexation between polymer blend and $MnBr_2$ is confirmed by XRD and optical studies. SEM micrographs ensure the formation of homogeneous composite films.

$MnBr_2$ loaded samples showed higher thermal stability than pure PVA/Cs blend. Activation energies for thermal decomposition derived by Broido equation showed negligible changes that exclude bond weakening effects in the blend after complexation with $MnBr_2$.

Absorption studies in the UV-Vis region reveal that the optical transition in all samples is direct allowed, and the optical energy gap decreased from 5.4 eV to 4.7 eV upon loading of $MnBr_2$ (5%) in the composites.

DC conductivity measurements confirmed that all samples were insulators at ambient temperature, although its conductivity increases by the addition of $MnBr_2$ to the blend matrix. Moreover, the temperature dependence of DC conductivity for all samples showed two thermally activated regions and the activation energies for both regions were calculated.

Frequency dependence of AC conductivity for different $MnBr_2$ loaded samples obeys the universal dynamic response, and an insulator to semiconductor change takes place upon increase of frequency (from 10^{-9} to 10^{-6} Ω^{-1} cm^{-1}).

The dielectric constant ε' of pure blend at ambient temperature is higher than that reported in literature for both pure chitosan and pure PVA and increases with increasing $MnBr_2$ content. Dehydration of samples results in a significant decrease in both the ε' and ε'' at ambient temperature, but ε' values are still higher than other PVA/Cs blend-metal salt composites. We suggest that these composites may be used in high dielectric constant applications.

Declaration of Conflicting Interests

The Authors declare that there is no conflict of interest

References

[1] Plastic Pollution - Our World in Data, https://ourworldindata.org/plastic-pollution (accessed April 20, 2020).

[2] Song JH, Murphy RJ, Narayan R, et al. Biodegradable and compostable alternatives to conventional plastics. *Philosophical Transactions of the Royal Society B: Biological Sciences* 2009; 364: 2127–2139.

[3] Li W, Zhao X, Huang Z, et al. Nanocellulose fibrils isolated from BHKP using ultrasonication and their reinforcing properties in transparent poly (vinyl alcohol) films. *Journal of Polymer Research* 2013; 20: 1–7.

[4] Pawde SM, Deshmukh K. Characterization of polyvinyl alcohol/gelatin blend hydrogel films for biomedical applications. *Journal of Applied Polymer Science* 2008; 109: 3431–3437.

[5] Abou-Aiad THM, Abd-El-Nour KN, Hakim IK, et al. Dielectric and interaction behavior of chitosan/polyvinyl alcohol and chitosan/polyvinyl pyrrolidone blends with some antimicrobial activities. *Polymer* 2006; 47: 379–389.

[6] Srinivasa PC, Ramesh MN, Kumar KR, et al. Properties and sorption studies of chitosan-polyvinyl alcohol blend films. *Carbohydrate Polymers* 2003; 53: 431–438.

[7] Sokker HH, Abdel Ghaffar AM, Gad YH, et al. Synthesis and characterization of hydrogels based on grafted chitosan for the controlled drug release. *Carbohydrate Polymers* 2009; 75: 222–229.

[8] Chuang WY, Young TH, Yao CH, et al. Properties of the poly(vinyl alcohol)/chitosan blend and its effect on the culture of fibroblast in vitro. *Biomaterials* 1999; 20: 1479–1487.

[9] Casey LS, Wilson LD. Investigation of Chitosan-PVA Composite Films and Their Adsorption Properties. *Journal of Geoscience and Environment Protection* 2015; 3: 78–84.

[10] RiandeEvaristo, Daz-Calleja Ricardo. *Electrical properties of polymers*. Marcel Dekker, 2004.

..

[11] Buraidah MH, Arof AK. Characterization of chitosan/PVA blended electrolyte doped with NH 4I. *Journal of Non-Crystalline Solids* 2011; 357: 3261–3266.

[12] Rathod SG, Bhajantri RF, Ravindrachary V, et al. Ionic conductivity and dielectric studies of LiClO 4 doped poly(vinylalcohol)(PVA)/chitosan(CS) composites . *Journal of Advanced Dielectrics* 2014; 04: 1450033.

[13] Hanafy TA. Dielectric relaxation and alternating-current conductivity of gadolinium-doped poly(vinyl alcohol). *Journal of Applied Polymer Science* 2008; 108: 2540–2549.

[14] Joshi GM, Cuberes MT. The DC bias function of electrical characterization of PVA inducted nickel chloride composite film. Ionics 2013; 19: 947–950.

[15] de Oliveira HP, dos Santos MVB, dos Santos CG, et al. Preparation and electrical and dielectric characterization of PVA/PPY blends. In: *Materials Characterization*. 2003, pp. 223–226.

[16] Plancha MJC, Rangel CM, Sequeira CAC. ac conductivity of polymer complexes formed by poly (ethylene oxide) and nickel chloride. *Solid State Ionics* 1992; 58: 3–7.

[17] CCP14 Homepage - Tutorials and Examples - LMGP suite for Windows by Jean Laugier and Bernard Bochu, http://www.ccp14.ac.uk/tutorial/lmgp/ (accessed April 20, 2020).

[18] Sudarsanan K. Manganesebromidetetrahydrate. *Acta Crystallographica* Section B *Structural Crystallography and Crystal Chemistry* 1975; 31: 2720–2721.

[19] Chen C-H, Wang F-Y, Mao C-F, et al. Studies of chitosan. I. Preparation and characterization of chitosan/poly(vinyl alcohol) blend films. *Journal of Applied Polymer Science* 2007; 105: 1086–1092.

[20] Naveen Kumar HMP, Prabhakar MN, Venkata Prasad C, et al. Compatibility studies of chitosan/PVA blend in 2% aqueous acetic acid solution at 30 °c. *Carbohydrate Polymers* 2010; 82: 251–255.

[21] Hodge RM, Edward GH, Simon GP. Water absorption and states of water in semicrystalline poly(vinyl alcohol) films. *Polymer* 1996; 37: 1371–1376.

[22] Elashmawi IS, Elsayed NH, Altalhi FA. The changes of spectroscopic, thermal and electrical properties of PVDF/PEO containing lithium nanoparticles. *Journal of Alloys and Compounds* 2014; 617: 877–883.

[23] Sheha EM, Nasr MM, El-Mansy MK. The role of MgBr2 to enhance the ionic conductivity of PVA/PEDOT: PSS polymer composite. *Journal of Advanced Research* 2015; 6: 563–569.

[24] Tawansi A, Ayad MI, Abdel- Razek EM. Effect of valence electron spin polarization on the physical properties of CuCl2- filled poly(vinylidene fluoride) as a microwave modulator. *Journal of Applied Polymer Science* 1999; 72: 771–781.

[25] Kadir MFZ, Majid SR, Arof AK. Plasticized chitosan-PVA blend polymer electrolyte based proton battery. *Electrochimica Acta* 2010; 55: 1475–1482.

[26] Mallakpour S, NezamzadehEzhieh A. Preparation and characterization of chitosan-poly(vinyl alcohol) nanocomposite films embedded with functionalized multi-walled carbon nanotube. *Carbohydrate Polymers* 2017; 166: 377–386.

[27] Lewandowska K. Miscibility and thermal stability of poly(vinyl alcohol)/chitosan mixtures. *Thermochimica Acta* 2009; 493: 42–48.

[28] Tsuchiya Y, Sumi K. Thermal decomposition products of poly(vinyl alcohol). Journal of Polymer Science Part A-1: *Polymer Chemistry* 1969; 7: 3151–3158.

[29] Yao F, Wu Q, Lei Y, et al. Thermal decomposition kinetics of natural fibers: Activation energy with dynamic thermogravimetric analysis. *Polymer Degradation and Stability* 2008; 93: 90–98.

[30] Cazón P, Vázquez M, Velazquez G. Composite films of regenerate cellulose with chitosan and polyvinyl alcohol: Evaluation of water adsorption, mechanical and optical properties. *International Journal of Biological Macromolecules* 2018; 117: 235–246.

[31] Vegt AK van der. *From polymers to plastics*. 2006; 268.

[32] Bower DI. Infrared dichroism, polarized fluorescence and Raman spectroscopy. In: Structure and Properties of Oriented Polymers. Springer Netherlands, 1997, pp. 181–233.

[33] Mistrik J, Kasap S, Ruda HE, et al. Optical properties of electronic materials: fundamentals and characterization. In: Springer Handbooks. Springer, 2017, p. 1.

[34] Abdolrahimi M, Seifi M, Ramezanzadeh MH. Study the effect of acetic acid on structural, optical and mechanical properties of PVA/chitosan/MWCNT films. *Chinese Journal of Physics* 2018; 56: 221–230.

[35] Andrady AL, Torikai A, Kobatake T. Spectral sensitivity of chitosan photodegradation. *Journal of Applied Polymer Science* 1996; 62: 1465–1471.

[36] Tauc J. Amorphous and Liquid Semiconductors. Springer US, 1974.

[37] Wood DL, Tauc J. Weak absorption tails in amorphous semiconductors. *Physical Review* B 1972; 5: 3144–3151.

[38] Mott NF (Nevill F, Davis EA (Edward A. Electronic processes in non-crystalline materials, Clarendon Press, 1971.

[39] Krstić J, Spasojević J, Radosavljević A, et al. Optical and structural properties of radiolytically in situ synthesized silver nanoparticles stabilized by chitosan/poly(vinyl alcohol) blends. *Radiation Physics and Chemistry* 2014; 96: 158–166.

[40] Mansour AF, Ahmed RM, Bassyouni AH, et al. Optical properties of gamma-irradiated ST/MMA copolymer. *International Journal of Polymeric Materials and Polymeric Biomaterials* 2007; 56: 207–226.

[41] Ali HM. Characterization of a new transparent-conducting material of ZnO doped ITO thin films. physica status solidi (a) 2005; 202: 2742–2752.

[42] El-Sayed S, Abel-Baset T, Elfadl AA, et al. Effect of nanosilica on optical, electric modulus and AC conductivity of polyvinyl alcohol/polyaniline films. *Physica B: Condensed Matter* 2015; 464: 17–27.

[43] Guirguis OW, Moselhey MTH. Optical study of poly(vinyl alcohol)/hydroxypropyl methylcellulose blends. *Journal of Materials Science* 2011; 46: 5775–5789.

[44] Polu AR, Kumar R, Kumar KV. Ionic conductivity and electrochemical cell studies of new Mg2+ ion conducting PVA/PEG based polymer blend electrolytes. *Advanced Materials Letters* 2012; 3: 406–409.

[45] Jez-Campos JBG, Prokhorov E, Iuna-Bárcenas G, et al. Dielectric relaxations of chitosan: The effect of water on the α-relaxation and the glass transition temperature. *Journal of Polymer Science Part B: Polymer Physics* 2009; 47: 2259–2271.

[46] Abu-Abdeen M, Saber O, Mazher J, et al. An effective and novel approach for enhancement of the oxidative thermal stability of multiwalled carbon nanotubes loaded polymer blend. *Journal of Thermoplastic Composite Materials.* Epub ahead of print 2019. DOI: 10.1177/0892705719830757.

[47] Bhavani S, Pavani Y, Ravi M, et al. Structural and Electrical Properties of Pure and NiCl₂Doped PVA Polymer Electrolytes. *American Journal of Polymer Science* 2013; 3: 56–62.

[48] Elliott SR. Frequency-dependent conductivity in ionically and electronically conducting amorphous solids. *Solid State Ionics* 1994; 70–71: 27–40.

..

[49] Lanfredi S, Gênova DHM, Brito IAO, et al. Structural characterization and Curie temperature determination of a sodium strontium niobate ferroelectric nanostructured powder. *Journal of Solid State Chemistry* 2011; 184: 990–1000.

[50] Raja V, Sharma AK, Rao VVRN. Impedance spectroscopic and dielectric analysis of PMMA-CO-P4VPNO polymer films. *Materials Letters* 2004; 58: 3242–3247.

[51] Deshmukh K, Ahamed MB, Sadasivuni KK, et al. Graphene oxide reinforced polyvinyl alcohol/polyethylene glycol blend composites as high-performance dielectric material. *Journal of Polymer Research* 2016; 23: 1–13.

[52] Nogales A, Ezquerra TA, Rueda DR, et al. Influence of water on the dielectric behaviour of chitosan films. *Colloid and Polymer Science* 1997; 275: 419–425.

[53] Brandrup Polymer Handbook | PDF | Polymerization | Polymers, https://www.scribd.com/document/243225535/Brandrup-Polymer-Handbook-pdf (accessed January 6, 2022).

[54] Bower DI. *An Introduction to Polymer Physics*. Epub ahead of print May 30, 2002. DOI: 10.1017/CBO9780511801280.

[55] Barber P, Balasubramanian S, Anguchamy Y, et al. Polymer Composite and Nanocomposite Dielectric Materials for Pulse Power Energy Storage. *Materials* 2009; 2: 1697–1733.

[56] Mohanapriya MK, Deshmukh K, Ahamed MB, et al. Zeolite 4A Filled Poly (3, 4-ethylenedioxythiophene): (polystyrenesulfonate) (PEDOT: PSS) And Polyvinyl Alcohol (PVA) Blend Nanocomposites As High-k Dielectric Materials For Embedded Capacitor Applications. *International Association of Advanced Materials* 2016; 7: 996–1002.